

# Journal of Materials Chemistry A

Accepted Manuscript



This is an *Accepted Manuscript*, which has been through the Royal Society of Chemistry peer review process and has been accepted for publication.

*Accepted Manuscripts* are published online shortly after acceptance, before technical editing, formatting and proof reading. Using this free service, authors can make their results available to the community, in citable form, before we publish the edited article. We will replace this *Accepted Manuscript* with the edited and formatted *Advance Article* as soon as it is available.

You can find more information about *Accepted Manuscripts* in the [Information for Authors](#).

Please note that technical editing may introduce minor changes to the text and/or graphics, which may alter content. The journal's standard [Terms & Conditions](#) and the [Ethical guidelines](#) still apply. In no event shall the Royal Society of Chemistry be held responsible for any errors or omissions in this *Accepted Manuscript* or any consequences arising from the use of any information it contains.

## Mn doped quantum dots sensitized solar cells with power conversion efficiency exceeding 9%

Jin Wang<sup>†</sup>, Yan Li<sup>†</sup>, Qing Shen<sup>‡,§</sup>, Takuya Izuishi<sup>‡</sup>, Zhenxiao Pan<sup>†</sup>, Ke Zhao<sup>†</sup>, and Xinhua Zhong<sup>†,\*</sup>

<sup>†</sup>Key Laboratory for Advanced Materials, Institute of Applied Chemistry, East China University of Science and Technology, Shanghai 200237, China

<sup>‡</sup>Department of Engineering Science, the University of Electro-Communications, 1-4-1 Chofugaoka, Chofu, Tokyo 182-8585, Japan

<sup>§</sup>Japan Science and Technology Agency (JST), 4-1-8 Honcho Kawaguchi, Saitama 332-0012, Japan

Email: zhongxh@ecust.edu.cn

Tel/Fax: (+86) 21 6425 0281

## Abstract

Transition metal ion (especially  $\text{Mn}^{2+}$ ) doping has been proven to be an effective approach to modify the intrinsic photo-electronic properties of semiconductor quantum dots (QDs). However, previous works of direct growth Mn doped QDs on  $\text{TiO}_2$  film electrode at room temperature renders the potential of Mn dopant not fully demonstrated in quantum dot sensitized solar cells (QDSCs). Herein, Mn doped  $\text{CdSe}_{0.65}\text{Te}_{0.35}$  QDs (simplified as Mn:QD) were pre-synthesized via “growth doping” strategy at high temperature. QD-sensitized photoanode with the configuration of  $\text{TiO}_2/\text{Mn:QD}/\text{Mn:ZnS}/\text{SiO}_2$  was prepared and corresponding cell devices were constructed with use of  $\text{Cu}_2\text{S}/\text{brass}$  counter electrodes and polysulfide electrolyte together with the reference cells with photoanode configurations of  $\text{TiO}_2/\text{Mn:QD}/\text{ZnS}/\text{SiO}_2$ ,  $\text{TiO}_2/\text{QD}/\text{Mn:ZnS}/\text{SiO}_2$ , and  $\text{TiO}_2/\text{QD}/\text{ZnS}/\text{SiO}_2$ , respectively. Photovoltaic performance results indicate that the  $\text{TiO}_2/\text{Mn:QD}/\text{Mn:ZnS}/\text{SiO}_2$  cells exhibit the best photovoltaic performance among all the studied cell devices with power conversion efficiency (PCE) for champion cell of 9.40% ( $J_{\text{sc}} = 20.87 \text{ mA}/\text{cm}^2$ ,  $V_{\text{oc}} = 0.688 \text{ V}$ ,  $\text{FF} = 0.655$ ) under AM 1.5 G one full sun illumination, which is among the best results for QDSCs. The open circuit voltage decay (OCVD), impedance spectroscopy (IS) and transient absorption (TA) characteristics confirm that the  $\text{Mn}^{2+}$  dopant can suppress charge recombination and improve the photovoltage and PCE of the resulting cells.

## 1. Introduction

Increasing demand for energy and depletion of fossil fuels force the exploration of alternative clean regenerative energy. The development of photovoltaic devices has opened up new opportunities for utilizing solar energy.<sup>1,2</sup> In recent years, the emergency of quantum dot sensitized solar cells (QDSCs) is perceived as one of the most promising candidates in low-cost third-generation solar cells.<sup>3-5</sup> Compared with other photovoltaic techniques, QDSCs exhibit various intrinsic advantages, such as solution processability, high absorption coefficient and tunable band-gap. Furthermore, multiple exciton generation possibility propels the theoretical power conversion efficiency (PCE) of QDSCs have the potential to beyond the Shockley–Queisser limit of 32%.<sup>6,7</sup> However, despite many efforts, QDSCs still suffer from moderate PCE with less than 10%.<sup>8-17</sup> An important reason for this moderate efficiency is the inferior optoelectronic properties of QD sensitizers.

A promising strategy to modify the intrinsic property of QDs is to introduce transition metal ion dopants such as  $\text{Mn}^{2+}$ . The dopant creates new electronic states in the host material, thus alters the charge separation and recombination dynamics. In addition, this dopant is both spin and orbital forbidden resulting in a long lifetime in a range of microseconds to milliseconds, which facilitates the long-lived photo-generated carriers.<sup>18-21</sup> In 2012, Kamat and co-workers pioneered the concept of Mn-doped CdS/CdSe QDSCs and pushed the PCE of QDSCs beyond 5% for the first time.<sup>22</sup> Since then, extensive efforts have been paid on the introduction of Mn dopant in QD sensitizers,<sup>22-29</sup> and/or in passivation/barrier layers<sup>30-33</sup> on sensitized photoanode for improving the performance of QDSCs. For example, Meng *et al.* designed  $\text{CuInS}_2/\text{Mn-doped CdS}$  QDSCs and obtained a PCE of 5.38%;<sup>23</sup> Cao *et al.* explored the Mn-doped CdSe QDSCs and achieved a PCE of 6.33%;<sup>25</sup> Kim *et al.* developed the CdS/CdSe/Mn-doped ZnSe QDSCs with a PCE of 5.67%.<sup>30</sup> It is noted that in these works, the dopant  $\text{Mn}^{2+}$  is generally introduced in the QD sensitizers through mixing  $\text{Mn}^{2+}$  with the corresponding cation aqueous solution constituting the target QD in the process of successive ionic layer adsorption and reaction (SILAR)<sup>22-23,26-33</sup> or chemical bath deposition (CBD)<sup>24-25</sup> for the direct growth of QD sensitizers on  $\text{TiO}_2$  film electrodes at room temperature. While, the adopted SILAR or CBD technique for loading QD sensitizer suffers from the disadvantages of broad size distribution and undesired surface defects. Compared with the SILAR or CBD deposition approaches, the postsynthesis assembly route has been confirmed to be a promising method to attain the monodispersed QDs with higher crystallinity, narrower size distribution, and tailored surface states.<sup>12-17</sup>

Regretfully, few works have been taken to utilize the pre-prepared Mn-doped QDs in the construction of QDSCs. Very recently, Bhattacharyya *et al.* successfully adopted the pre-synthesized Mn-doped CdS in the construction of QDSCs.<sup>34</sup> The limited light harvesting range of the CdS host material together with improper QD deposition approach in that work lead to a rather low PCE of 2.1%. Hence, the development of a host material with near-infrared absorption is necessary for the achievement of high efficiency in QDSCs. Among various QDs, the CdSe<sub>0.65</sub>Te<sub>0.35</sub> QDSCs with ZnS/SiO<sub>2</sub> barrier layers have achieved a PCE as high as 8.55%.<sup>12</sup> Hence, the CdSe<sub>0.65</sub>Te<sub>0.35</sub> QDs could be an ideal host material for Mn dopant in the construction of high efficiency QDSCs. Especially, different from the Mn doped CdS QD system, where Mn<sup>2+</sup> excited states are lowest in energy and lie in the band gap of host QDs, for the Mn doped CdSeTe QD system, the Mn excited states lie outside the band gap of CdSeTe QDs. In this system, the Mn impurities act as electron trap centers in doped CdSeTe QDs for the photoexcited electron. The long-lived high-energy doping levels of Mn impurities thus provide an advantage of retarding charge recombination and result in improved performance of the cell devices. Previous experimental results confirmed that charge recombination dynamics was found to be much slower in the Mn doped CdSe QD system as compared with that in the undoped system.<sup>35</sup>

Herein, we report the construction of high efficiency QDSCs with use of pre-prepared high-quality Mn-doped CdSe<sub>0.65</sub>Te<sub>0.35</sub> (noted as Mn:CdSeTe henceforth) colloidal QDs, which were tethered on TiO<sub>2</sub> film electrode by the recently reported capping ligand-induced self-assembly technique.<sup>36-38</sup> Colloidal Mn:CdSeTe QDs with near-infrared absorption was prepared through a “growth doping” strategy at high temperature. After deposition of Mn:CdSeTe QD on TiO<sub>2</sub> film electrode, Mn-doped ZnS/SiO<sub>2</sub> passivation layers were sequentially overcoated around the QD sensitized photoanode. For comparison, QDSCs based on plain CdSeTe QD sensitizer and plain ZnS passivation layer were also constructed. The Mn dopant in both QD sensitizer and ZnS passivation layer favors the enhancement of photocurrent, photovoltage, and consequently PCE of the resultant cell devices. The champion QDSC based on Mn:CdSeTe QD sensitizer and Mn:ZnS passivation layer exhibits a PCE of 9.40% (with  $J_{sc} = 20.87 \text{ mA/cm}^2$ ,  $V_{oc} = 0.688 \text{ V}$ ,  $FF = 0.655$ ) under AM 1.5 G one full sun illumination, which is among the best performances for QDSCs.

## 2. Experimental section

### Chemicals.

Cadmium oxide (99.99%), manganese acetate tetrahydrate ( $\text{Mn}(\text{OAc})_2 \cdot 4\text{H}_2\text{O}$ , 98%), selenium powder (200 mesh, 99.99%), tellurium powder (200 mesh, 99.99%), oleylamine (OAm, 97%), and trioctylphosphine (TOP, 90%) were purchased from Aldrich. Thioglycolic acid (TGA, 97%), and oleic acid (OA, 90%) were obtained from Alfa. Paraffin liquid (chemical grade) was purchased from Shanghai chemical reagents company, China. All reagents were used without further purification.

### Synthesis and water-solubilization of Mn:CdSeTe QDs.

The oil-soluble Mn:CdSeTe QDs were synthesized according to literature method with slight modification.<sup>39</sup> In a typical procedure, 0.35 mL of 0.1 M Te and 0.65 mL of 0.1 M Se precursor solutions, obtained by dissolving Te or Se in paraffin and TOP (v/v, 3:1) at 300 or 200 °C under  $\text{N}_2$ , were loaded in a 50 mL round-bottom flask. Then 5.0 mL of 0.1 M  $\text{Cd}(\text{OA})_2$  stock solution, obtained by dissolving CdO in oleic acid and paraffin (v/v, 1:3) at 250 °C under  $\text{N}_2$ , was added with stirring. Afterward, the resulting reaction mixture was degassed under vacuum at 110 °C for 10 min to form an orange solution. The reaction system was further heated to 200 °C. At this temperature, 0.5 mL of 0.01 M  $\text{Mn}(\text{OA})_2$  precursor solution, obtained by dissolving  $\text{Mn}(\text{OAc})_2 \cdot 4\text{H}_2\text{O}$  in oleic acid and paraffin (v/v, 1:4) at 150 °C under  $\text{N}_2$ , was injected into the flask with stirring, and the reaction temperature was further heated to 320 °C and stayed at this temperature for 20 min. Then, the reaction temperature was lowered to 260 °C, and 2.0 mL of OAm was added into the reaction system and stayed for another 6 min before removing the heater and cooling to 60 °C. Then 10.0 mL of hexane–methanol (v/v, 1:1) was used as the extraction solvent to separate the formed QDs from byproducts and unreacted precursors if present. The Mn content in the resulting CdSeTe QDs is 0.56% related to Cd. For simplicity, both the Mn:CdSeTe and Mn:QD are referred to this composition henceforth. With the variation of the nominal amount of Mn precursor in the synthesis, Mn content in the obtained QD can be tuned correspondingly. The detailed results for Mn contents in the obtained Mn:QD samples determined by ICP-AES (Inductively Coupled Plasma-Atomic Emission Spectrometry) corresponding to nominal Mn contents used in the synthesis are shown in Table S1 of the Electronic Supplementary Information (ESI).

The process of preparation of  $\text{CdSe}_{0.65}\text{Te}_{0.35}$  QDs is identical to that for Mn:CdSeTe as mentioned above but without the step of injection of Mn stock solution. A standard literature

method was adopted for the water-solubilization of the initial oil-soluble Mn:CdSeTe, and CdSeTe QDs with use of thioglycolic acid (TGA) as phase transfer agent.<sup>40</sup> Experimental details are available in Electronic supplementary information (ESI).

### **Fabrication of QDSCs.**

TiO<sub>2</sub> mesoporous film electrodes with thickness of  $15.0 \pm 0.5 \mu\text{m}$  (9.0  $\mu\text{m}$  transparent layer combined with 6.0  $\mu\text{m}$  light scattering layer) were prepared according to literature method.<sup>41</sup> For the deposition of Mn:CdSeTe (or CdSeTe) QDs onto the TiO<sub>2</sub> film electrode, TGA-capped QD aqueous dispersions are pipetted onto the electrodes and stayed for 6 h. The QD-sensitized photoanodes were then overcoated by Mn:ZnS (or ZnS)/SiO<sub>2</sub> double passivation layers according to previous reports.<sup>12</sup> To be specific, the Mn:ZnS passivation layer were overcoated by immersing QD-sensitized photoanodes into a methanol solution containing 0.1 M Zn(OAc)<sub>2</sub> and 0.01 M Mn(OAc)<sub>2</sub>, and 0.1 M Na<sub>2</sub>S aqueous solution for 1 min/dip alternately for four cycles, and then coated sequentially with SiO<sub>2</sub> passivation layer by soaking the electrodes in 0.01 M tetraethyl orthosilicate ethanol solution for 2 h. The counter electrodes were fabricated by immersing brass in HCl solution at 70°C for 30 min, then washed with deionized water and dried. The liquid electrolyte were prepared by dissolving 2.0 M Na<sub>2</sub>S and 2.0 M S in deionized water. The devices were constructed by assembling the counter electrodes and the working electrodes in Sandwich structure and separating by a 50- $\mu\text{m}$  thickness scotch spacer. In order to ensure the reliability of the evaluation data, five cells were prepared and measured in parallel under each condition.

### **Characterization.**

The composition for the Mn:QD was measured using an ICP-AES (Thermo Elemental IRIS 1000) (dissolved with HCl–HNO<sub>3</sub>). The electron paramagnetic resonance (EPR) spectra were recorded on a Bruker EMX-10/12 X-band digital EPR spectrometer. *J–V* curves of devices were measured under an AM 1.5 G solar simulator with intensity of 100 mW/cm<sup>2</sup> and sweep rate of 60 mV/s. Before each test, calibration was carried by a NREL standard Si solar cell. The active area of cells was 0.2354 cm<sup>2</sup>, which was defined by a black metallic mask. The spectra of IPCE were recorded by a Keithley 2000 multimeter. Impedance spectroscopy (IS) were recorded on an impedance analyzer (Zahner, Zennium) in dark conditions at forward bias ranging from 0 to –0.6V, applying a 20 mV AC sinusoidal signal over the constant applied bias with the frequency range of 1 MHz to 0.1 Hz. Open circuit voltage decay (OCVD) were performed on the same Zahner workstation and the cells were illuminated by a white LED with intensity of 100 mW/cm<sup>2</sup>, then voltage signal were recorded after switching off the

light. The X-ray Photoelectron Spectroscopy (XPS) were characterized by an ESCALAB 250Xi spectrometer, using focused monochromatized Al  $K_{\alpha}$  radiation ( $h\nu = 1486.7$  eV). Transient absorption (TA) setups were used to characterize the samples in the femtosecond (fs) time range. The laser source was a titanium/sapphire laser (CPA-2010, Clark-MXR Inc.) with wavelength of 775 nm, repetition rate of 1 kHz, and pulse width of 150 fs. The light was separated into two parts: one as a probe pulse, the other as a pump light to pump an optical parametric amplifier (OPA) (a TOAPS from Quantronix) to generate light pulses with wavelength tunable from 290 nm to 3  $\mu$ m. In this study, a pump light wavelength of 470 nm and a probe beam wavelength of 580 nm were used.

### 3. Results and discussion

#### Synthesis and optical properties of Mn:CdSeTe QDs.

CdSe<sub>0.65</sub>Te<sub>0.35</sub> QDs were chosen as the model sensitizer due to the high PCE of 8.5% obtained from this QD sensitizer based QDSCs.<sup>12</sup> For the synthesis of Mn:CdSeTe QDs, a modified “growth doping” strategy has been adopted.<sup>42,43</sup> In this strategy, small sized CdSeTe QD hosts were primarily formed below 200 °C, then the Mn<sup>2+</sup> dopant precursor (Mn(OA)<sub>2</sub>) was introduced and doping occurred through surface binding. With increase of reaction temperature and the continuous growth of QD host, the adsorbed dopant Mn was encapsulated by further epitaxial growth of CdSeTe. The successful doping of Mn into the CdSeTe QD host was confirmed by the ICP-AES measurement, which gave a Mn content of 0.56% related to Cd under the nominal Mn/Cd ratio of 5% used in the synthesis. Experimental results indicate that Mn content in the resulting Mn:CdSeTe QDs is dependent on the initial Mn amount used in the synthesis (detailed results shown in Table S1). The observed less Mn content in the formed product should be ascribed to the “self-purification” mechanism that the energetically unfavorable Mn impurity inside the QD lattice is prone to be ejected out from the host QDs.<sup>44</sup> The photovoltaic measurement results indicate that Mn:CdSeTe QDs with 0.56% Mn/Cd ratio gives the best performance for the resulting cell devices as discussed below. When the nominal Mn content is greater than 5%, the device performance decreases gradually. The PL spectra corresponding to different Mn contents in the obtained QD products as well as the average photovoltaic performances of the corresponding cell devices are shown in Figure S1 and Table S2. For convenience, the Mn:CdSeTe QD is referred specially to the Mn content of 0.56% in this work. Besides, The UV/Vis absorption spectrum of TGA-capped CdSeTe QDs aqueous solution is also shown in Figure S1, which shows no significant change before and after phase transfer. The incorporation of Mn dopant in CdSeTe QD was further confirmed by the electron paramagnetic resonance (EPR) characterization with corresponding spectrum shown in Figure S2. A relative large splitting constant (A) value of 87.6 Gauss was

observed for the obtained Mn:CdSeTe QD sample. This result suggests that  $\text{Mn}^{2+}$  is located close to the surface of host QDs rather than in the internal lattice site of the host QDs.<sup>34, 45</sup>

Absorption spectrum of the Mn:CdSeTe QD dispersion (Figure 1a) in toluene show nearly an identical spectral profile to that of un-doped CdSeTe QD solution with absorption edge extending to near infrared region of about 820 nm. The identical spectral profile indicates that the Mn dopant does not change the electronic structure of the host QDs. While, the intensity of photoluminescence (PL) emission peak (Figure 1a) from Mn:CdSeTe is significantly stronger than that from CdSeTe QDs. The increased PL emission indicates the better suppression of non-radiative recombination in the Mn-doped QD in comparison with plain CdSeTe QDs, and this is favorable for the photovoltaic performance of the resulting cell devices as discussed below. These results indicate clearly that the capping ligand protects the QD better in the system of Mn:CdSeTe QDs, therefore results in less density of surface trap defects and higher PL QY. The better capping ligand protection may be derived from the crystal growth control by the Mn impurity. The intrinsic mechanism for the influence of Mn impurity on the capping ligand protection effect in the QD growth process is unclear currently, and further explorations are needed. The observed sole PL emission peak located at 840 nm should be derived from the host CdSeTe as the Mn d-electron emission should be located at yellow-orange spectral window of 580-600 nm.<sup>46-50</sup> The absence of the Mn dopant emission is reasonable since the Mn 3d-orbital energy level is located outside the band gap of the CdSeTe host QDs.<sup>39</sup> The TEM images (Figure 1d, e) together with the representative HRTEM images in the insets show a nearly identical average particle size of 5.6 nm for both the Mn:CdSeTe and CdSeTe QDs, but the size distribution for Mn:CdSeTe QDs is more narrow than that for CdSeTe QD (with relative standard deviation of 4% vs. 8%). This finding indicates that the Mn impurity could effectively narrow the size distribution since the impurities can interfere the ongoing crystal growth process and assist the formation of the structural architecture.<sup>51,52</sup>

#### **Enhanced chemical stability of Mn:CdSeTe QDs.**

It is well accepted that the stability of a QDSC device is strongly dependent on the QDs' stability.<sup>10</sup> The QDs that containing Te element is sensitive to oxygen. This leads to an unpredictable change in electronic and optical properties.<sup>53</sup> Surprisingly and importantly, the Mn:CdSeTe QDs show a significantly improved stability compared to that of plain CdSeTe QDs. Experimental results indicate that the TGA-capped Mn:CdSeTe QD aqueous solution remained clear for 30 days' storage at ambient condition and no observable variation was observed for the absorption spectra as shown in Figure 1b; while agglomeration and precipitation occurred in the counterpart CdSeTe QD aqueous solution after stored for 10 days

(as shown in the inset of Figure 1b). All these results imply that the Mn: CdSeTe QDs show a superior chemical stability to that of CdSeTe QDs. The observed higher stability of the Mn: CdSeTe QDs in compared to plain CdSeTe QDs should be ascribed to the better capping ligand encapsulating effect. The better capping ligand encapsulating may be derived from the crystal growth control by the Mn impurity. Regrettably, the intrinsic mechanism for the dependence of crystal growth on Mn impurity is unclear currently, and this needs further exploration. The enhanced chemical stability of the obtained Mn: CdSeTe QDs paves a way for the construction of QDSCs with extended performance lifetime. As expected, the Mn: QD/Mn: ZnS based QDSCs showed better stability in comparison with that of QD/ZnS based ones. Experimental results (Figure S4) indicate that the PCE values for the QD/ZnS cells start to decline gradually after 24 h, and reach to about 70% of the initial values in a course of 36 h irradiation by one full sun intensity; while the Mn: QD/Mn: ZnS cells keeps nearly the best performance in the whole period. It is noted that Cu<sub>2</sub>S/FTO counter electrodes, made by depositing Cu<sub>2</sub>S nanocrystal paste on FTO were used in the performance stability tests.<sup>54</sup>

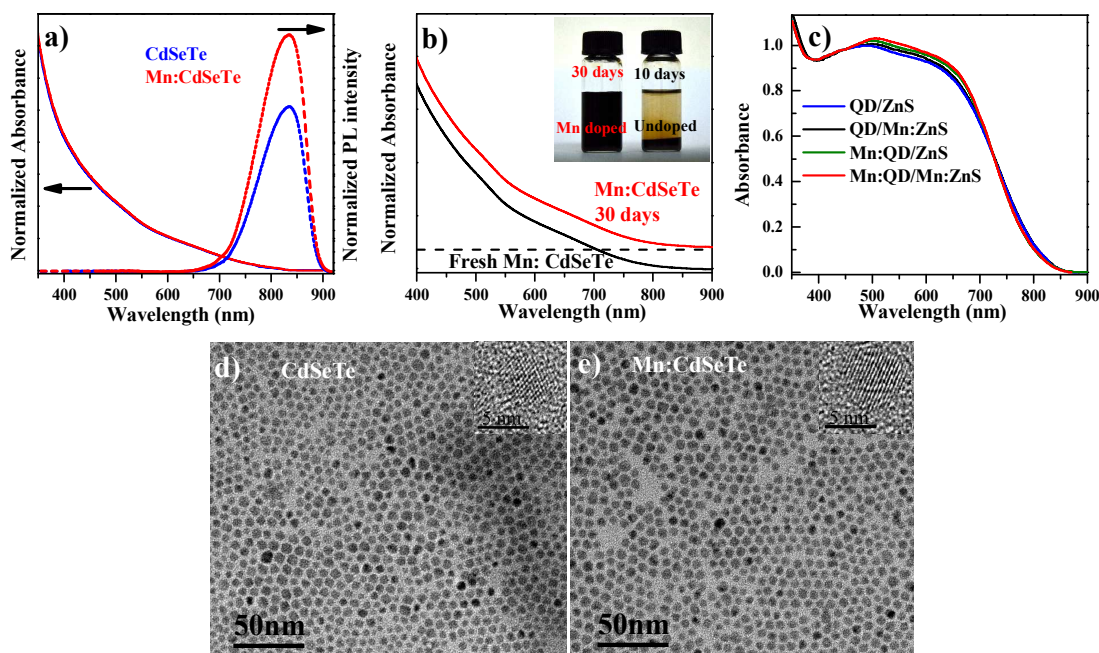


**Figure 1.** Optical spectra and TEM images of CdSeTe QD, derivative Mn: CdSeTe QD dispersions in toluene (a) Absorption and PL emission spectra ( $\lambda_{\text{ex}} = 400 \text{ nm}$ ) of QD dispersions, respectively. (b) Absorption spectra of TGA-capped Mn: CdSeTe QD aqueous dispersion before and after 30 days storage. Inset: Photographs of Mn: CdSeTe (left) and CdSeTe (right) QD aqueous dispersions after storage for certain period. (c) Absorption spectra of QD sensitized photoanode films with different configurations. (d-e) TEM images of

CdSeTe and Mn:CdSeTe QDs.

### **Fabrication of QD-sensitized photoanodes.**

For sensitization of TiO<sub>2</sub> film electrodes by QDs, the initial OAm-capped oil-soluble Mn:CdSeTe QDs was transferred into bifunctional linker molecule TGA-capped water-soluble QDs through phase transfer process.<sup>40</sup> Then the QD-sensitized electrodes were obtained via the capping ligand-induced self-assembly process by pipetting the obtained TGA-capped QD aqueous solution onto TiO<sub>2</sub> film electrode and stayed for 6 h.<sup>40</sup> This sensitization approach can offer a dense coverage of QD on TiO<sub>2</sub> film electrode as proven in previous reports.<sup>38</sup> For comparison, the CdSeTe QD sensitized TiO<sub>2</sub> film electrodes were also prepared through the identical procedure. In order to reduce the charge recombination at the photoanode/electrolyte interface, thin ZnS/SiO<sub>2</sub> passivation layers were sequentially overcoated around the QD-sensitized TiO<sub>2</sub> film electrode according to the standard literature method.<sup>12</sup> In replacing the ZnS layer, Mn:ZnS layer was overcoated around the sensitized electrode by mixing Mn<sup>2+</sup> with the Zn<sup>2+</sup> aqueous solution under optimized Mn/Zn ratio of 1:10 in the process of overcoating ZnS layer. Meanwhile, different Mn/Zn ratios have been investigated in the overcoating of Mn:ZnS layer, and the influence on photovoltaic performance is given in Table S3 of SI. Following the ZnS, or Mn:ZnS overcoating layer, SiO<sub>2</sub> layer was overcoated sequentially according to literature method.<sup>12</sup> Overall, four types of photoanodes corresponding to four types of QDSCs were prepared, which include: Mn:CdSeTe sensitized photoanode with ZnS/SiO<sub>2</sub> passivation layer (simplified as Mn:QD/ZnS); Mn:CdSeTe sensitized photoanode with Mn:ZnS/SiO<sub>2</sub> passivation layer (simplified as Mn:QD/Mn:ZnS); CdSeTe sensitized photoanode with ZnS/SiO<sub>2</sub> passivation layer (simplified as QD/ZnS); and CdSeTe sensitized photoanode with Mn:ZnS/SiO<sub>2</sub> passivation layer (simplified as QD/Mn:ZnS). It is noted that in these abbreviations, the composition of QD is CdSe<sub>0.65</sub>Te<sub>0.35</sub>; the Mn content in Mn:QD is 0.56%; the Mn/Zn ratio in Mn:ZnS layer is 1:10; SiO<sub>2</sub> layer is omitted, but it is present in all these samples.

UV/Vis absorption spectra (Figure 1c) of the prepared QD-sensitized TiO<sub>2</sub> film electrodes (composing 6.0 μm transparent layer without scattering layers) were measured. The absorption edge of the QD-sensitized TiO<sub>2</sub> photoanode is consistent with that of QD dispersion in water. It is found that the Mn:QD/Mn:ZnS photoanode film shows the greatest absorbance, while the QD/ZnS shows the least absorbance. This indicates that greater loading amount was achieved in the Mn:QD sensitized photoanode. The cause may be derived from

the improved monodispersity of the Mn: CdSeTe QDs related to CdSeTe as discussed above. The improved monodispersity favors the penetration of QD particle into the mesoporous channel in the TiO<sub>2</sub> substrate. The improved loading amount of QD sensitizers in the case of Mn doped QDs means greater light harvesting capability and higher photocurrent in the cell devices. This would be verified by the photovoltaic results as discussed below. Furthermore, the Mn dopant in ZnS layer also has slightly effect on the enhancement of light harvesting in comparison with plain ZnS layer. These results reveal that the construction of Mn:QD/Mn:ZnS photoanodes have the potential to improve light harvesting capability and achieve higher photocurrent in the resulting cell devices.

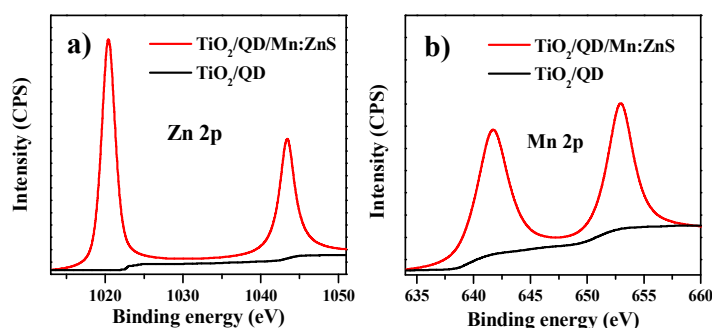


**Figure 2.** X-ray photoelectron spectra (XPS) (a) Zn 2p and (b) Mn 2p peaks derived from TiO<sub>2</sub>/CdSeTe/Mn:ZnS samples.

In the overcoating of Mn:ZnS layer around QD sensitized photoanode, the Mn<sup>2+</sup> and Zn<sup>2+</sup> ions mixture aqueous solution was employed. The existence and valance states of Mn in the photoanode were characterized by X-ray photoelectron spectroscopy (XPS). It is noted that in order to eliminate the interference of Mn in CdSeTe QDs, plain CdSeTe QDs were used in the preparation of samples for XPS measurement. Figure 2 displays the XPS spectra of the CdSeTe QDs sensitized photoanode coated with Mn:ZnS and the uncoated counterpart. Compared with the XPS spectrum of the reference TiO<sub>2</sub>/QD sample, the two binding energy peaks at 641 eV and 653 eV appear in that of TiO<sub>2</sub>/QD/Mn:ZnS sample, which indicate that the presence of the Mn<sup>2+</sup>; furthermore, two peaks at 1020 eV and 1043 eV were observed for TiO<sub>2</sub>/QD/Mn:ZnS sample that is assigned to the Zn 2p binding energy verifying the presence of the Zn<sup>2+</sup> expected for Mn:ZnS. These results indicate that a Mn:ZnS passivation layer have been formed during the process of SILAR.

### TA measurement.

To elaborate the influence of Mn dopant on electron injection rate from QD sensitizer to TiO<sub>2</sub> substrate, the femtosecond (fs) transient absorption (TA) technique was employed. In the TA

measurements, QD sensitizer with different configurations, including QD/ZnS, QD/Mn:ZnS, Mn:QD/ZnS, Mn:QD/Mn:ZnS, were deposited on insulating SiO<sub>2</sub> or TiO<sub>2</sub> substrate with identical procedure for sensitization of photoanodes. After the excitation by pump light, the QDs undergo charge separation, and the transient bleaching signal are recorded simultaneously. Figure 3 shows the TA decay curves of the four types of QD sensitizers deposited on TiO<sub>2</sub> or SiO<sub>2</sub> substrate, which correspond to kinetic traces of the charge carrier decay for the samples. It is observed that for all the studied QD sensitizers on insulator SiO<sub>2</sub> substrate, the recovery rate of the bleaching is rather slow. This is because the insulating properties of SiO<sub>2</sub> prevents the injection of photo-generated electron from QD to SiO<sub>2</sub> substrate, and therefore the charge recombination in QDs is dominated by the internal recombination including excitonic state and defect states. However, the recovery rate of bleaching for QDs on TiO<sub>2</sub> substrate is much faster since an additional fast electron-transfer route from QD to TiO<sub>2</sub> substrate exists in this case. The TA kinetics can be fitted well using a biexponential function, and the average lifetimes (listed in Table 1) of the photoexcited carriers can be obtained according to eq (1).

$$\tau_{av} = (A_1\tau_1^2 + A_2\tau_2^2)/(A_1\tau_1 + A_2\tau_2) \quad (1)$$

Where  $\tau_1$  and  $\tau_2$  refer to are the lifetimes, and  $A_1$  and  $A_2$  are the relative weights of the two decay components. It can be found that  $\tau_{av}$  values increased remarkably when the Mn dopant is present in CdSeTe QDs or in ZnS passivation layer. These results reveal that the Mn dopant can reduce the intrinsic defects of CdSeTe QDs. These observations are also in good agreement with the PL properties as mentioned above. The electron injection rate constant  $k_{et}$  can be obtained from eq (2).<sup>55</sup>

$$k_{et} = 1/\tau_{av(QD/TiO_2)} - 1/\tau_{av(QD/SiO_2)} \quad (2)$$

As listed in Table 1, the  $k_{et}$  decreases slightly with the presence of Mn dopant in sensitizer system. In this sense, Mn dopant has a trade-off effect: on one hand reducing internal recombination, and on the other hand retarding electron injection rate. It is noted that the  $k_{et}$  of  $1.6 \times 10^{10} \text{ s}^{-1}$  for the TiO<sub>2</sub>/Mn:QD/Mn:ZnS system is fast enough for the efficient electron injection into TiO<sub>2</sub> substrate since the competing recombination rates are usually less than  $10^9 \text{ s}^{-1}$ .<sup>5,56</sup>

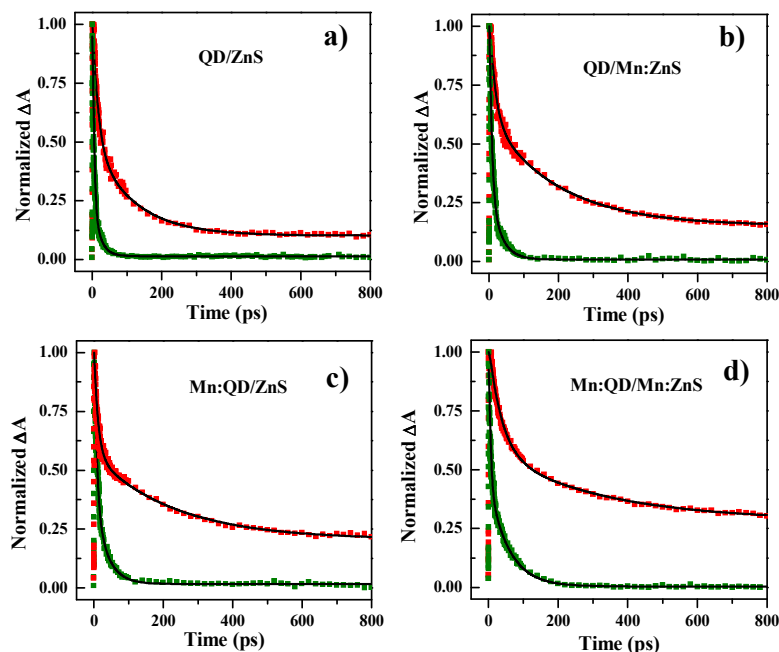


**Figure 3.** TA characterization in picosecond time scale. Kinetic traces of the excitonic decay (recorded at 580 nm) of (a) QD/ZnS, (b) QD/Mn:ZnS, (c) Mn:QD/ZnS and (d) Mn:QD/Mn:ZnS QDs deposited on SiO<sub>2</sub> (red scatters) and TiO<sub>2</sub> substrates (olive scatters) for a time scale up to 800 ps. The bold lines represent the corresponding biexponential fit.

**Table 1.** Fitting Results of the TA Responses with Biexponential Function and Calculated Average Lifetime Using Eq 1 as Well as Electron Injection Rate Calculated Using Eq 2

Samples	$\tau_1$ (ps)	$\tau_2$ (ps)	$A_1$	$A_2$	$\tau_{av}$ (ps)	$k_{et}$ ( $\times 10^{10} \text{ s}^{-1}$ )
SiO <sub>2</sub> /QD/ZnS	16.30	118.16	0.52	0.40	102.48	
SiO <sub>2</sub> /QD/Mn:ZnS	16.39	195.45	0.46	0.46	181.70	
SiO <sub>2</sub> /Mn:QD/ZnS	12.26	230.92	0.36	0.41	218.43	
SiO <sub>2</sub> /Mn:QD/Mn:ZnS	36.49	316.44	0.30	0.46	274.42	
TiO <sub>2</sub> /QD/ZnS	3.23	18.64	0.85	0.29	13.41	6.48
TiO <sub>2</sub> /QD/Mn:ZnS	5.75	29.15	0.83	0.34	21.60	4.08
TiO <sub>2</sub> /Mn:QD/ZnS	6.97	34.37	0.67	0.39	27.25	3.21
TiO <sub>2</sub> /Mn:QD/Mn:ZnS	4.43	55.85	0.62	0.45	50.79	1.60

**Photovoltaic performance.**

The solar cells were fabricated by assembling the sensitized photoanodes and Cu<sub>2</sub>S/brass counter electrode with use of polysulfide electrolyte. The current density–voltage ( $J$ – $V$ ) curves of champion cells for four types of QDSCs are presented in Figure 4a, and the average photovoltaic parameters of all cells are summarized in Table 2 (detailed parameters for each device are shown in Table S4 and Figure S3), together with the results for champion cells of each type of cells. As expected, the average short-circuit current ( $J_{sc}$ ) for the cells with Mn dopant is higher than those without Mn dopant, and the Mn:QD/Mn:ZnS cells exhibit the highest  $J_{sc}$  (20.83 mA/cm<sup>2</sup>) among all the studied four types of cells (20.43–20.72 mA/cm<sup>2</sup> for other cells). The higher  $J_{sc}$  in Mn:QD/Mn:ZnS cells is benefited from the greater light harvesting capacity as indicated by the absorption spectra of the sensitized film electrodes in Figure 1c. Meanwhile, the absorbance ratios among different sensitized photoanodes are consistent with the corresponding  $J_{sc}$  ratios. The obtained  $J_{sc}$  from  $J$ – $V$  measurement is very close to the integrated  $J_{sc}$  according to the incident-photon to conversion efficiency (IPCE) spectra as shown in Figure 4b with corresponding value in the range of 19.68 to 20.48 mA/cm<sup>2</sup>. Besides the enhancement of  $J_{sc}$ , a distinct improvement of open circuit voltage ( $V_{oc}$ ) has also been observed for cell devices with Mn dopant. This clearly strengthens the advantages of the adopted post-synthesis assembly route for QD deposition. Similarly, the Mn:QD/Mn:ZnS cells exhibit the highest  $V_{oc}$  value (0.685 V) among all the studied cells (0.652–0.670 V for other cells). While, the Mn dopant has no significant influence on fill factor (FF) of the corresponding cell devices. Benefited from the enhanced  $J_{sc}$  and  $V_{oc}$ , the solar cell with Mn dopant in either QD sensitizer or ZnS passivation layer show higher PCEs. Furthermore, the contribution by the Mn dopant in QD sensitizer in PCE enhancement is about two times greater than that by the Mn dopant in ZnS layer (increase of 5.1% vs 2.8%). The champion Mn:QD/Mn:ZnS cell exhibits the PCE of 9.40% (with  $V_{oc}$  = 0.687 V,  $J_{sc}$  = 20.88 mA/cm<sup>2</sup>, and FF = 65.5%), which is one of the highest efficiency in QDSCs ever reported to date.<sup>10–12</sup> It is noted that the QD/ZnS cells show the average PCE of 8.44%, which is close to previous results with the same configuration.<sup>12</sup>

**Table 2.** Photovoltaic parameters of QDSCs corresponding to different electrodes. Average solar cell parameters and standard deviations for the 5 different device preparations under 1 sun illumination. The numbers in parentheses represent the values obtained for the champion cells.

QDSCs	$J_{sc}$ (mA/cm <sup>2</sup> )	$V_{oc}$ (V)	FF (%)	PCE (%)
QD/ZnS	20.43(20.46)	0.652(0.654)	63.3(63.9)	8.44±0.07(8.55)
QD/Mn:ZnS	20.57(20.60)	0.666(0.668)	63.7(64.1)	8.72±0.06(8.82)
Mn:QD/ZnS	20.72(20.79)	0.670(0.674)	64.2(64.5)	8.91±0.09(9.04)
Mn:QD/Mn:ZnS	20.83(20.88)	0.685(0.687)	64.7(65.5)	9.23±0.11(9.40)

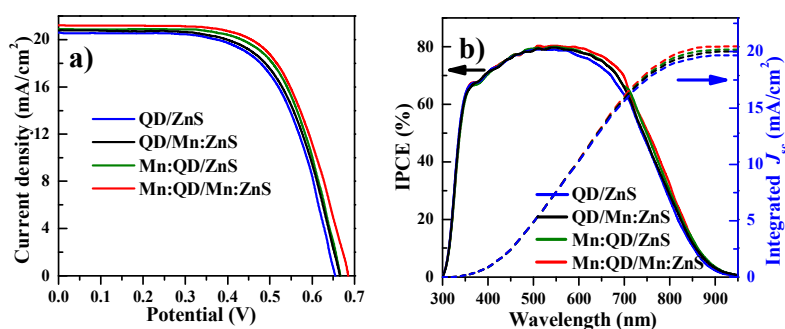


**Figure 4.** Solar cell performance. (a)  $J$ - $V$  curves for the champion cells. (b) IPCE spectra and integrated  $J_{sc}$ .

#### Open circuit voltage decay (OCVD).

In order to elaborate the effect of Mn dopant in improving performance of the resultant cell devices, open circuit voltage decay (OCVD) and impedance spectroscopy measurement have been applied. The OCVD technique can provide the information about electron recombination processes, i.e. photo-generated electrons recombination with oxidized species in the redox couple in electrolyte media. The measured voltage decay signals for studied cell devices after switching off the illumination were shown in Figure 5a. From it, we can find that the solar cells based on Mn: CdSeTe QDs (i.e. Mn:QD/Mn:ZnS and Mn:QD/ZnS cells) exhibited a slower decay rate than cells based on plain CdSeTe QDs (i.e. QD/Mn:ZnS and QD/ZnS cells).

It has been established that  $V_{oc}$  decay rate can be translated into the electron lifetime ( $\tau_n$ ) under open circuit condition (Figure 5b) according to eq (3),<sup>57</sup> and the obtained  $\tau_n$  can directly reflect the charge recombination inside devices.

$$\tau_n = -(k_B T/e)(dV_{oc}/dt)^{-1} \quad (3)$$

From Figure 5b, a linear decrease in  $\tau_n$  is observed with the increase of voltage for all the cell devices under open-circuit conditions. Furthermore, the  $\tau_n$  values for Mn: CdSeTe QD sensitized cells are greater than those for the plain CdSeTe QD sensitized ones. The variation trend of  $\tau_n$  values in different cell devices is in accordance with that of  $V_{oc}$  and PCE as discussed above. Among the investigated cell samples, the  $\tau_n$  value for Mn:QD/Mn:ZnS device is the greatest one, which is about four times higher than that for the QD/ZnS cells. These results demonstrate the effectiveness of Mn dopant in QD sensitizer in suppressing recombination.

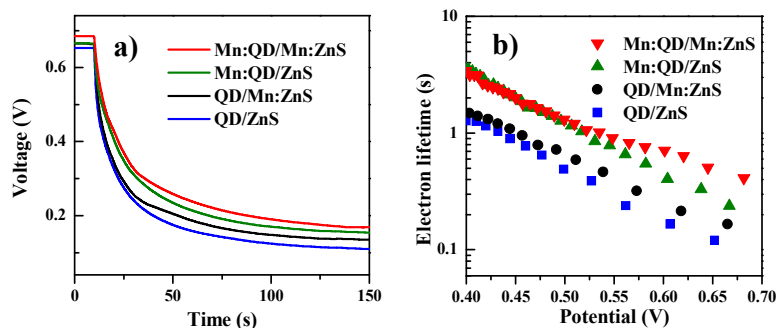


**Figure 5.** (a) Open circuit voltage decay (OCVD), and (b) extracted electron lifetime as a function of  $V_{oc}$ .

### Impedance spectroscopy (IS).

To further clarify the effect of Mn dopant in improving the performance of the resulting photovoltaic devices, impedance spectroscopy (IS) measurement was performed to obtain the electrical resistance and recombination dynamics of various devices. IS measurements were performed in dark conditions at forward bias ranging from 0 V to an bias voltage higher than  $V_{oc}$  with frequency range of 1 MHz to 0.1 Hz. The detailed Nyquist plots for all cells under different bias are given in Figure S5. Standard fitting models and equivalent circuit were used to analyze the obtained IS data.<sup>8, 58-62</sup> The extracted chemical capacitance  $C_{\mu}$ , and

recombination resistance  $R_{\text{rec}}$  from the obtained IS measurement data are shown in Figure 6a, b, respectively. The observed similar  $C_{\mu}$  value for all cell devices implies that the dopant in either QD sensitizers or in ZnS passivation layer does not alter the conduction band edge of  $\text{TiO}_2$  electron collector. However, the difference in the recombination resistance  $R_{\text{rec}}$  is distinct for cells with or without Mn dopant (Figure 6b). Similar to the variation trend of  $\tau_n$ , it is observed that the  $R_{\text{rec}}$  values for Mn: CdSeTe QD sensitized cells are greater than those for the plain CdSeTe QD sensitized ones, and the  $R_{\text{rec}}$  value for Mn:QD/Mn:ZnS device is the greatest one (about 3 times greater than that for QD/ZnS cells). The greater  $R_{\text{rec}}$  value in the cells corresponds to the reduced charge recombination rate in the cells since  $R_{\text{rec}}$  is inversely proportional to the recombination rate.<sup>61</sup> Moreover, the calculated electron lifetime  $\tau_n$  from the IS results ( $\tau_n = R_{\text{rec}} \times C_{\mu}$ ) also exhibits a relative higher value for the cells with Mn dopant than those without Mn dopant (1.46s vs 0.45s). In addition, the trend of  $\tau_n$  results extracted from IS measurements are consistent with that from OCVD measurements. To distinguish the recombination difference among different cell devices, the Nyquist plots of various solar cells at forward bias of  $-0.60$  V, which is close to the  $V_{\text{oc}}$  of cell devices, are shown in Figure 6d, and the extracted IS parameters using the equivalent circuit shown in the inset of Figure 6d are collected in Table S5.<sup>8</sup> It is found that the transport resistance ( $R_w$ ) is increased slightly by doping Mn in both QD sensitizer (26.89 vs 29.51  $\Omega$ ) and ZnS passivation layer (26.89 vs 33.15  $\Omega$ ). This increase indicates that electron transport rate in  $\text{TiO}_2$  film electrode is reduced by Mn doping. While the ratio of  $R_{\text{ct}}/R_w$  increases with Mn doping (increasing from 3.8 to 8.0), especially for the case of Mn doping in QD sensitizer. This demonstrates that both Mn doping in ZnS barrier layer and in QD sensitizer restrains the recombination reaction rate at photoanode/electrolyte interface, and results in better charge collection efficiency in the photoanode.<sup>62</sup> It is clear that the Mn:QD/Mn:ZnS cells exhibit the greatest  $R_{\text{ct}}/R_w$  value (8.0) among all the investigated cell devices, and therefore have the best performance.

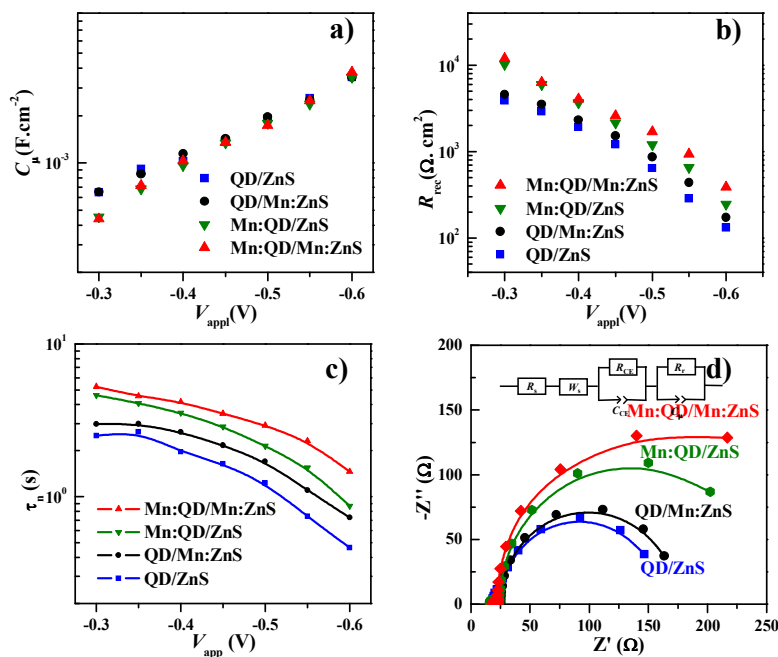


**Figure 6.** IS characterization of QDSCs with different configurations. Dependence of (a) chemical capacitance  $C_{\mu}$ , (b) recombination resistance  $R_{rec}$ , (c) electron lifetime  $\tau_n$  with different applied voltages. (d) Nyquist plots of the solar cells under bias voltage of -0.6 V.

#### 4. Conclusions

In summary, a new route for Mn-doped QDSCs has been designed and developed, and a PCE of 9.40% has been achieved from the champion Mn:QD/Mn:ZnS cell device. Experimental results indicate that in the crystal growth process, the presence of Mn dopant can narrow the size distribution of host QDs, and the enhanced monodispersity is favorable for improving loading amount of QD on TiO<sub>2</sub> film electrode, and therefore brings forward higher photocurrent of the resultant cell device. All the optical spectra, TA, OCVD, and IS measurement results confirm that the presence of Mn dopant can reduce trap states in QD sensitizers, and can consequently suppress charge recombination and improve photovoltage and PCE of the resulting cell devices. In addition, the contribution for performance improvement from the Mn dopant in QD sensitizer is more significant than that from the Mn dopant in ZnS passivation layer. All these features reveal that the Mn-doped QD sensitizer is one of promising candidates for the construction of high efficiency QDSCs.

## Acknowledgements

This research is supported by the Natural Science Foundation of China (nos. 21421004, 91433106), and the Fundamental Research Funds for the Central Universities in China.

† **Electronic supplementary information (ESI) available:** Ligand Exchange with Water-Soluble TGA. Average photovoltaic parameters of 5 cells in parallel for Mn:CdSeTe/ZnS based QDSCs corresponding to the different mole ratio of Mn in QDs. The dependence of photovoltaic performance of Mn:QD/Mn:ZnS QDSCs on the nominal Mn/Zn ratio in the ZnS passivation layer.  $J-V$  curves and the corresponding parameters of various types of devices (each group has 5 devices in parallel). Nyquist curves under different bias voltages and impedance values at a  $-0.6$  V forward bias for all kinds of solar cells.

## References

- 1 K. W. J. Barnham, M. Mazzer and B. Clive, *Nat. Mater.*, 2006, **5**, 161.
- 2 M. He, D. Zheng, M. Wang, C. Lin and Z. Lin, *J. Mater. Chem. A*, 2014, **2**, 5994.
- 3 P. V. Kamat, *Acc. Chem. Res.*, 2012, **45**, 1906.
- 4 J. L. Duan, H. H. Zhang, Q. W. Tang, B. L. He and L. M. Yu, *J. Mater. Chem. A*, 2015, **3**, 17497.
- 5 G. Hodes, *J. Phys. Chem. C*, 2008, **112**, 17778.
- 6 O. E. Semonin, J. M. Luther, S. Choi, H.-Y. Chen, J. Gao, A. J. Nozik and M. C. Beard, *Science*, 2011, **334**, 1530.
- 7 A. J. Nozik, M. C. Beard, J. M. Luther, M. Law, R. J. Ellingson and J. C. Johnson, *Chem. Rev.*, 2010, **110**, 6873.
- 8 K. Y. Yan, L. X. Zhang, J. H. Qiu, Y. C. Qiu, Z. L. Zhu, J. N. Wang and S. H. Yang, *J. Am. Chem. Soc.*, 2013, **135**, 9531.
- 9 A. Sahasrabudhe, S. Bhattacharyya, *Chem. Mater.*, 2015, **27**, 4848.
- 10 C. M. Chuang, P. R. Brown, V. Bulovic and M. G. Bawendi, *Nat. Mater.*, 2014, **13**, 796.
- 11 Z. Ning, O. Voznyy, J. Pan, S. Hoogland, V. Adinolfi, J. Xu, M. Li, A. R. Kirmani, J. P. Sun, J. Minor, K. W. Kemp, H. Dong, L. Rollny, A. Labelle, G. Carey, B. Sutherland, I. Hill, A. Amassian, H. Liu, J. Tang, O. M. Bakr and E. H. Sargent, *Nat. Mater.*, 2014, **13**, 822.
- 12 K. Zhao, Z. X. Pan, I. Mora-Seró, E. Cánovas, H. Wang, Y. Song, X. Q. Gong, J. Wang, M. Bonn, J. Bisquert and X. H. Zhong, *J. Am. Chem. Soc.*, 2015, **137**, 5602.
- 13 Z. X. Pan, H. Zhang, K. Cheng, Y. M. Hou, J. L. Hua and X. H. Zhong, *ACS Nano*, 2012, **6**, 3982.
- 14 J. Wang, I. Mora-Seró, Z. X. Pan, K. Zhao, H. Zhang, Y. Y. Feng, G. Yang, X. H. Zhong and J. Bisquert, *J. Am. Chem. Soc.*, 2013, **135**, 15913.
- 15 Z. X. Pan, I. Mora-Seró, Q. Shen, H. Zhang, Y. Li, K. Zhao, J. Wang, X. H. Zhong and J. Bisquert, *J. Am. Chem. Soc.*, 2014, **136**, 9203.
- 16 S. Jiao, Q. Shen, I. Mora-Seró, J. Wang, Z. X. Pan, K. Zhao, Y. Kuga, X. H. Zhong and J. Bisquert, *ACS Nano*, 2015, **9**, 908.
- 17 W. J. Li, Z. X. Pan and X. H. Zhong, *J. Mater. Chem. A*, 2015, **3**, 1649.
- 18 R. N. Bhargava, D. Gallagher, X. Hong and A. Nurmikko, *Phys. Rev. Lett.*, 1994, **72**, 416.
- 19 R. Beaulac, P. I. Archer, S. T. Ochsenein and D. R. Gamelin, *Adv. Funct. Mater.*, 2008, **18**, 3873.
- 20 D. J. Norris, A. L. Efros and S. C. Erwin, *Science*, 2008, **319**, 1776.
- 21 Y. T. Dong, J. Choi, H. K. Jeong and D. H. Son, *J. Am. Chem. Soc.*, 2015, **137**, 5549.
- 22 P. K. Santra and P. V. Kamat, *J. Am. Chem. Soc.*, 2012, **134**, 2508.
- 23 J. H. Luo, H. Y. Wei, Q. L. Huang, X. Hu, H. F. Zhao, R. Yu, D. M. Li, Y. H. Luo and Q. B. Meng, *Chem. Commun.*, 2013, **49**, 3881.

- 24 J. J. Tian, L. L. Lv, C. B. Fei, Y. J. Wang, X. G. Liu and G. Z. Cao, *J. Mater. Chem. A*, 2014, **2**, 19653.
- 25 C. J. Liu, H. Tang, J. Li, W. Z. Li, Y. H. Yang, Y. M. Li and Q. Y. Chen, *RSC Adv.*, 2015, **5**, 35506.
- 26 H. J. Kim, H. D. Lee, C. S. S. P. Kumar, S. S. Rao, S. H. Chung and D. Punnoose, *New J. Chem.*, 2015, **39**, 4805.
- 27 P. K. Santra and Y. S. Chen, *Electrochimi. Acta*, 2014, **146**, 654.
- 28 D. Punnoose, S. S. Rao, S. K. Kim and H. J. Kim, *RSC Adv.*, 2015, **5**, 33136.
- 29 C. V. V. M. Gopi, M. Venkata-Haritha, S. K. Kim and H. J. Kim, *Dalton Trans.*, 2015, **44**, 630.
- 30 C. V. V. M. Gopi, M. V. Haritha, S. K. Kim and H. J. Kim, *Nanoscale*, 2015, **7**, 12552.
- 31 S. S. Rao, I. K. Durga, C. V. Tulasi-Varma, D. Punnoose, S. K. Kim and H. J. Kim, *Org. Electron.*, 2015, **26**, 200.
- 32 L. B. Yu, Z. Li, Y. B. Liu, F. Cheng and S. Q. Sun, *Appl. Surf. Sci.*, 2014, **309**, 255.
- 33 Z. Li, L. B. Yu, Y. B. Liu and S. Q. Sun, *Electrochimi. Acta*, 2015, **153**, 200.
- 34 G. Halder and S. Bhattacharyya, *J. Phys. Chem. C*, 2015, **119**, 13404.
- 35 T. Debnath, P. Maity, S. Maiti and H. N. Ghosh, *J. Phys. Chem. Lett.*, 2014, **5**, 2836.
- 36 W. J. Li and X. H. Zhong, *J. Phys. Chem. Lett.*, 2015, **6**, 796.
- 37 W. J. Li and X. H. Zhong, *Acta Phys. Sin.*, 2015, **64**, 038806.
- 38 H. Zhang, K. Cheng, Y. M. Hou, Z. Fang, Z. X. Pan, W. J. Wu, J. L. Hua and X. H. Zhong, *Chem. Commun.*, 2012, **48**, 11235.
- 39 Z. X. Pan, K. Zhao, J. Wang, H. Zhang, Y. Y. Feng and X. H. Zhong, *ACS Nano*, 2013, **7**, 5215.
- 40 J. W. Yang, T. Oshima, W. Oshima, Z. X. Pan, X. H. Zhong and Q. Shen, *J. Mater. Chem. A*, 2014, **2**, 20882.
- 41 Z. L. Du, H. Zhang, H. L. Bao and X. H. Zhong, *J. Mater. Chem. A*, 2014, **2**, 13033.
- 42 N. Pradhan, D. Goorskey, J. Thessing and X. G. Peng, *J. Am. Chem. Soc.*, 2005, **127**, 17586.
- 43 R. Buonsanti and D. J. Milliron, *Chem. Mater.*, 2013, **8**, 1305.
- 44 G. M. Dalpian and J. R. Chelikowsky, *Phys. Rev. Lett.*, 2006, **96**, 226802.
- 45 D. Magana, S. C. Perera, A. G. Harter, N. S. Dalal and G. F. Strouse, *J. Am. Chem. Soc.*, 2006, **128**, 2931.
- 46 N. Pradhan and X. G. Peng, *J. Am. Chem. Soc.*, 2007, **129**, 3339.
- 47 W. J. Zhang, Y. Li, H. Zhang, X. G. Zhou and X. H. Zhong, *Inorg. Chem.*, 2011, **50**, 10432.
- 48 R. S. Zeng, M. Rutherford, R. G. Xie, B. S. Zou and X. G. Peng, *Chem. Mater.*, 2010, **22**, 2107.
- 49 A. Nag, S. Sapra, C. Nagamani, A. Sharma, N. Pradhan, S. V. Bhat and D. D. Sarma, *Chem. Mater.*, 2007, **19**, 3252.
- 50 D. J. Norris, N. Yao, F. T. Charnock and T. A. Kennedy, *Nano Lett.*, 2001, **1**, 3.
- 51 L. J. Zu, D. J. Norris, T. A. Kennedy, S. C. Erwin and A. L. Efros, *Nano Lett.*, 2006, **6**, 334.
- 52 A. K. Guria, G. Prusty, B. K. Patra and N. Pradhan, *J. Am. Chem. Soc.*, 2015, **137**, 5123.

- 53 J. H. Bang and P. V. Kamat, *ACS Nano*, 2009, **3**, 1467.
- 54 H. Zhang, H. Bao and X. H. Zhong, *J. Mater. Chem. A*, 2015, **3**, 6557.
- 55 Q. Shen,; Y. Ogomi, S. K. Das, S. S. Pandey, K. Yoshino, K. Katayama, H. Momose, T. Toyoda and S. Hayase, *Phys. Chem. Chem. Phys.*, 2013, **15**, 14370.
- 56 H. M. Zhu, N. H. Song and T. Q. Lian, *J. Am. Chem. Soc.*, 2013, **135**, 11461.
- 57 A. Zaban, M. Greenshtein and J. Bisquert, *ChemPhysChem*, 2003, **4**, 859.
- 58 I. Mora-Seró, S. Gimenez, F. Fabregat-Santiago, R. Gomez, Q. Shen, T. Toyoda and J. Bisquert, *Acc. Chem. Res.*, 2009, **42**, 1848.
- 59 F. Fabregat-Santiago, G. Garcia-Belmonte, I. Mora-Seró and J. Bisquert, *Phys. Chem. Chem. Phys.*, 2011, **13**, 9083.
- 60 V. González-Pedro, X. Xu, I. Mora-Seró and J. Bisquert, *ACS Nano*, 2010, **4**, 5783.
- 61 M. Samadpour, P. P. Boix, S. Giménez, A. Irají Zad, N. Taghavinia, I. Mora-Seró and J. Bisquert, *J. Phys. Chem. C*, 2011, **115**, 14400.
- 62 M. Adachi, M. Sakamoto, J. Jiu, Y. Ogata and S. Isoda, *J. Phys. Chem. B*, 2006, **110**, 13872.

## Table of content (TOC)

### Mn doped quantum dots sensitized solar cells with power conversion efficiency exceeding 9%

Jin Wang, Yan Li, Qing Shen, Takuya Izuishi, Zhenxiao Pan, Ke Zhao, and Xinhua Zhong\*

